Changes in polarization dictate necessary approximations for modeling electronic deexcitation intensity: Application to x-ray emission

Subhayan Roychoudhury,[1,*] Leonardo A. Cunha,[2,3,†] Martin Head-Gordon,[2,3,‡] and David Prendergast[1,§]
[1]*The Molecular Foundry, Lawrence Berkeley National Laboratory, Berkeley, California 94720, USA*
[2]*Department of Chemistry, University of California Berkeley, California 94720, USA*
[3]*Chemical Sciences Division, Lawrence Berkeley National Laboratory, Berkeley, California 94720, USA*

(Received 19 December 2021; revised 30 June 2022; accepted 25 July 2022; published 17 August 2022)

Accurate simulation of electronic excitations and deexcitations are critical for complementing complex spectroscopic experiments and can provide validation to theoretical approaches. Using a generalized framework, we contrast the accuracy and validity of orbital-constrained and linear-response approaches that build upon Kohn-Sham density functional theory (DFT) to simulate emission spectra of electronic origin and propose an efficient approximation, named many-body x-ray emission spectroscopy or MBXES, for simulating such processes. We show analytically as well as with computed examples that for electronic (de)excitation leading to an appreciable change in polarization (i.e., density rearrangement), the adiabatic approximation in a response-based formalism will be inadequate for the calculation of oscillator strength. Thus, such a change (e.g., in the net electrostatic dipole moment of a finite system) can be used as a metric for evaluating the applicability of the adiabatic response-based approach and can be particularly valuable in x-ray emission spectroscopy. On the other hand, MBXES, the flexible method introduced in this paper, can compute oscillator strengths accurately at a much lower computational expense on the basis of two DFT-based self-consistent field calculations. Using illustrative examples of emission spectra, the efficacy of the MBXES method is demonstrated by comparison with its parent theory, orbital-optimized DFT, and with experiments.

DOI: 10.1103/PhysRevB.106.075133

I. INTRODUCTION

Investigating the electronic structure of materials is of paramount importance, not only to advance scientific understanding, but also from a technological perspective. Electronic structure is typically probed in terms of neutral or charged electronic excited states. A complete investigation of excited states involves the determination not only of the energies of the states but also of the transition probabilities for excitation (deexcitation) to (from) them. There are various experimental methods for this purpose, which provide opportunities to validate and advance theoretical efforts. For decades, density-functional theory (DFT) [1,2] has been the primary workhorse in electronic structure calculations [3–6]. Even though DFT is a ground-state theory, various techniques build upon DFT by leveraging different levels of approximation to probe electronic excited states [7–17]. The two main avenues for this, both of which are widely used in practice, are the response-based treatment, where a response function is evaluated indirectly by creating electron-hole (e-h) pairs in a reference state; and the orbital-constrained treatment, which models the target state using constrained non-Aufbau orbital occupancy.

In this paper we link these two disparate approaches within a generalized framework. For valence-to-core electronic transitions, we show analytically, as well as with computed examples, that within the computationally tractable adiabatic approximation, inaccuracy in the response-based approach is correlated with the change in the valence polarization due to the core ionization of the system. Additionally, working within the orbital-constrained approach, by modifying the state-of-the-art orbital-optimized DFT (ooDFT) formalism with physically motivated approximations, we propose a computational method for simulating nonresonant x-ray emission, with a focus on accurate calculation of the transition amplitude.

Electronic transitions, which can involve both the core and the valence electrons, typically span a wide energy range. In order to ensure tractability of our calculation, we focus on electronic deexcitations since this allows us to limit our attention to the occupied subspace only, offering appreciable computational advantage. Deexcitations can either be confined fully within the valence subspace, or involve valence-to-core transitions. Due to the availability of experimental data, the latter kind, which is experimentally accessible within the nonresonant x-ray emission spectroscopy (XES) technique, will be the primary focus of our computational demonstrations. Notably, since the goal of this work is the analysis of purely electronic deexcitations, additional effects which might influence the experimental spectra, e.g., the ionic vibrations present at finite temperature [18,19] (note that vibrational effects typically make the spectra smoother by

*roychos@tcd.ie
†leonardo.cunha@berkeley.edu
‡mhg@cchem.berkeley.edu
§dgprendergast@lbl.gov

introducing additional broadening [20] and can occasionally introduce new peaks [21]) have not been taken into account.

II. NONRESONANT X-RAY EMISSION FORMALISM

In non-resonant XES [22–25], spontaneous x-ray emission (or fluorescence) occurs from an initially core-ionized sample. As the core-excited system decays from an initial state Ψ_I with energy E_I to any possible final state Ψ_F with energy E_F, the emission intensity

$$I(\omega) \propto \sum_F (E_I - E_F)^4 |M^{I,F}|^2 \delta(\omega + E_F - E_I) \tag{1}$$

is recorded as a function of its frequency ω, where, denoting the many-body transition operator by $\hat{O}$, the transition matrix element is given by $M^{I,F} = \langle \Psi_F | \hat{O} | \Psi_I \rangle$. Therefore $|\Psi_\mathrm{I}\rangle$, i.e., the state prior to the x-ray emission process, can be represented by the lowest energy state of the positively charged system with a core hole on the excited atom. In our calculations, this is approximated by a single Slater determinant (SD) composed of Kohn-Sham (KS) orbitals obtained from a self-consistent field (SCF) DFT calculation, where one core orbital is constrained to be empty, which we denote as the zeroth orbital. One numerically stable approach to obtain this core-hole excited state directly is the maximum overlap method (MOM) [26]. If there are N electrons remaining in the system, then, denoting the creation operator for the jth initial-state orbital $\tilde{\phi}_j$ by $\tilde{a}_j^\dagger$, we can represent the SD as

$$|\Psi_\mathrm{I}\rangle = \left(\prod_{j=1}^{N} \tilde{a}_j^\dagger \right) |0\rangle \,. \tag{2}$$

The exact Fth final state [27] resulting from deexcitation (filling the zeroth orbital via $\tilde{a}_0^\dagger$) can then be formally expressed as

$$|\Psi_F^\mathrm{exact}\rangle = \left[\sum_{j=1}^{N} \alpha_j^F \tilde{a}_j \tilde{a}_0^\dagger |\Psi_\mathrm{I}\rangle \right] + \left[\sum_{l,m=1}^{N} \sum_{p=N+1}^{\mathrm{all}} \beta_{l,m,p}^F \tilde{a}_l \tilde{a}_m \tilde{a}_p^\dagger \tilde{a}_0^\dagger |\Psi_\mathrm{I}\rangle \right] + \cdots , \tag{3}$$

where α and β are expansion coefficients, and we use tildes to indicate that these initial state orbitals include a core hole. The terms inside the first (second) set of square brackets represent the terms obtained from $|\Psi_\mathrm{I}\rangle$ by single (double) substitutions, i.e., by creating one (two) e-h pair(s) in $|\Psi_\mathrm{I}\rangle$. The previously excited core orbital is indicated, as stated above, by subscript 0. Notably, beyond the singles term, i.e., in doubles and beyond, we start populating the unoccupied valence subspace of $|\Psi_\mathrm{I}\rangle$. However, only the singles can contribute to the transition-dipole matrix [28]

$$M_\mathrm{exact}^F = \left\langle \Psi_F^\mathrm{exact} | \hat{O} | \Psi_\mathrm{I} \right\rangle = \sum_{j=1}^{N} \left(\alpha_j^F\right)^* \langle \phi_0 | \hat{o} | \tilde{\phi}_j \rangle \,, \tag{4}$$

since for higher substitutions, the overlap with $\hat{O}\,|\Psi_\mathrm{I}\rangle$ vanishes. Here, $\hat{O}$ ($\hat{o}$) denotes the many-body (single-particle) transition operator, defined explicitly below.

III. XES WITHIN ADIABATIC LINEAR RESPONSE

Now, in principle, response-based frameworks, such as linear response time-dependent DFT (LR-TDDFT) and the Bethe-Salpeter equation, evaluate the absorption/emission spectra exactly from the imaginary part of the density-density response function χ—the change in electron density as a function of external potential. The complex problem of finding χ is mapped into that of diagonalizing a fictitious, typically non-Hermitian, two-particle Hamiltonian H^{2p}. Even though, strictly speaking, the response-based approaches do not offer any access to the wave functions, within the Tamm-Dancoff approximation [29], the final state is often approximated [30] by an eigenstate of H^{2p} and expressed as a linear combination of Slater determinants obtained by creating an e-h pair on the initial state $|\Psi_I\rangle$ (analogous to the configuration-interaction singles approach) as

$$\left|\Psi_F^\mathrm{Resp}\right\rangle = \sum_{j=1}^{N} \gamma_j^F \tilde{a}_j a_0^\dagger |\Psi_\mathrm{I}\rangle \,, \tag{5}$$

such that the corresponding transition amplitude

$$M_\mathrm{Resp}^F = \left\langle \Psi_F^\mathrm{Resp} | \hat{O} | \Psi_\mathrm{I} \right\rangle = \sum_{j=1}^{N} \left(\gamma_j^F\right)^* \langle \phi_0 | \hat{o} | \tilde{\phi}_j \rangle \tag{6}$$

is identical to that of a single-particle deexcitation from the auxiliary orbital

$$\left|\phi_F^\mathrm{Resp}\right\rangle = \sum_{j=1}^{N} \left(\gamma_j^F\right)^* |\tilde{\phi}_j\rangle \,. \tag{7}$$

In response-based approaches, the e-h interaction is encoded with the help of a kernel K, which, in its exact form, is time dependent. However, in the standard, computationally viable adiabatic approximation [15], this dynamic effect is ignored. Within this approximation, the number of accessible final states equals the number of e-h pairs that can be created on the initial state and each approximate final state is normalized [15]. The normalization constraint means that, unless all contributions beyond the singles vanish identically in Eq. (3) (which is possible only if the occupied valence subspace of $|\Psi_F^\mathrm{exact}\rangle$ has no overlap with the unoccupied subspace of $|\Psi_\mathrm{I}\rangle$), the set of coefficients $\{\gamma^F\}$ must differ from $\{\alpha^F\}$, resulting invariably in the relation $M_\mathrm{Resp}^F \neq M_\mathrm{exact}^F$.

This leads to the crucial inference that if there is appreciable difference between the valence occupied subspaces of the ground and the core-ionized state—if the valence electron density is significantly rearranged due, in this case, to the annihilation of the core hole in XES—then, adiabatic response-based approaches will inevitably incur errors in the oscillator strength. By definition, this rearrangement of the valence electronic density defines a polarization response due to the perturbation, which is proportional to the spatially nonlocal electronic susceptibility.

Since the susceptibility of a given ground state naturally invokes coupling to the unoccupied orbital subspace, the change

in the aforementioned response, i.e., the change in the valence polarization, serves as a useful metric for the validity of the adiabatic approximation in the response-based treatment. This metric can be particularly important in XES, since the annihilation of a localized core hole may easily result in a significant renormalization of the occupied orbitals, leading to a large change in polarization.

Notably, this argument does not preclude the exact time-dependent kernel from yielding the accurate oscillator strength, since, in this case, the requirement of normalization will not be applicable for $|\Psi_F^{\mathrm{Resp}}\rangle$. In other words, the inadequacy is a consequence of the adiabatic approximation, not of the response-based approach, which, in principle, calculates χ exactly. Note that, such valence-to-core deexcitations can help the formulation of accurate frequency-dependent kernels [31] by providing experimental data for verification of their efficacy.

This analytical conclusion can be demonstrated using the molecular examples shown in Fig. 1, where the polarization response is simply the change in the electrostatic dipole moment of the molecule. We compare the measured and simulated XES spectra of two small molecules (chloromethane [32] and phenol [33]), with calculations using DFT orbitals produced by the Q-CHEM code [34] using the ωB97M − V exchange-correlation functional [35] and the large aug-cc-pCVQZ basis set [36,37]. The energy convergence threshold was set to 10^{-8} a.u., and 10^{-14} a.u. was used as the threshold for screening two-electron integrals. The SG-2 standard quadrature grid is used for the DFT calculations which use the Pulay DIIS algorithm for convergence. A value of 10^{-8} a.u. is chosen as the threshold for the LR-TDDFT calculations.

Comparison with the experimental spectra reveals that the adiabatic LR-TDDFT spectrum is in good agreement for Cl $K\beta$ emission of CH_3Cl, which corresponds to a lower (1.43 D) change in the electrostatic dipole moment. However, for O $K\alpha$ emission of C_6H_5OH, the change is larger (3.01 D) and the mismatch with experiment is noticeable (particularly near 527 eV).

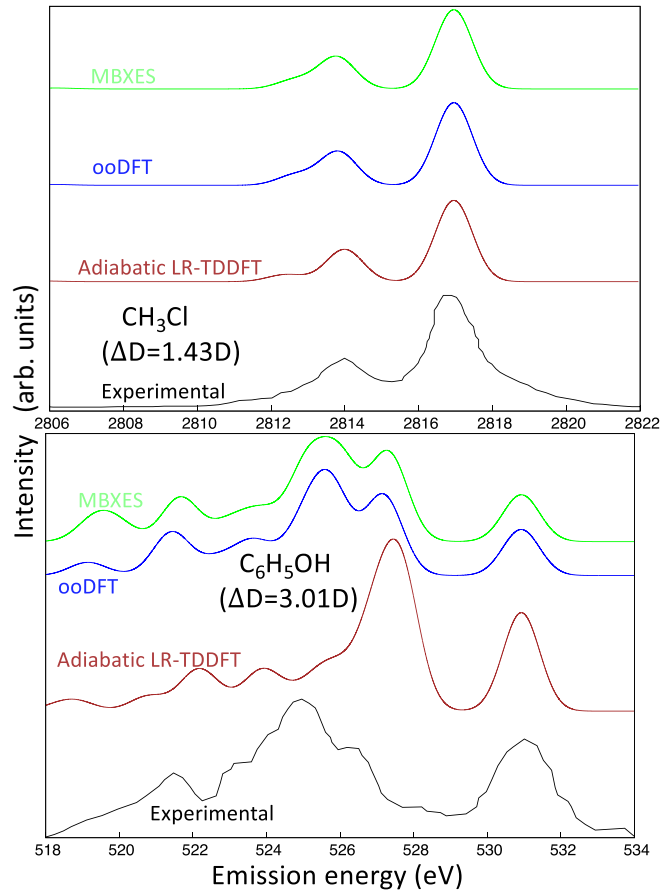

FIG. 1. X-ray emission spectra for (top) Cl $K\beta$ from chloromethane (CH_3Cl) and (bottom) O $K\alpha$ from phenol (C_6H_5OH) simulated using adiabatic LR-TDDFT (brown), ooDFT (blue), MBXES (green), and compared with experiment (black), from Refs [32] and [33], respectively. The associated change in dipole moment (ΔD) is indicated in each case. As detailed in the text, ΔD is a diagnostic for errors in LR-TDDFT arising from the adiabatic approximation, which is not required in ooDFT or MBXES (an approximation to ooDFT). A rigid shift is added to each simulated spectrum to align the highest-energy peak with the experiment

IV. XES WITHIN THE ORBITAL-CONSTRAINED APPROACH

A. General framework

Having characterized the shortcomings of the adiabatic response-based technique for simulating valence-to-core deexcitation intensity, we turn our attention to the orbital-constrained approach. Let us consider the general case of optical dipole transitions between many-body states, initial and final, comprising single-particle orbitals from distinct SCFs. The many-body transition operator can be written, with respect to the initial state, as

$$\hat{O} = \sum_{i,j} \langle \tilde{\phi}_j | \hat{o} | \tilde{\phi}_i \rangle \, \tilde{a}_j^\dagger \tilde{a}_i, \tag{8}$$

where the ordering of operations is deliberate and the sum runs over the entire single-particle Hilbert space of the initial state. These transitions are individually weighted by their single-particle dipole matrix elements: $\tilde{o}_{ji} = \langle \tilde{\phi}_j | \hat{o} | \tilde{\phi}_i \rangle$, where $\hat{o} = \epsilon \cdot \hat{\mathbf{r}}$ defines the electric field polarization and its interaction with the electronic position. Whether these transitions are allowed or not depends on the many-body state and its orbital occupations. We will work within the single Slater determinant approximation, where the N occupied orbitals that define the self-consistent field via the electron density can also define a many-body state, emergent from the vacuum, as

$$|\Psi\rangle = \prod_{i=1}^{N} a_i^\dagger \, |0\rangle \, , \tag{9}$$

where the creation and annihilation operators correspond to the orbitals of the relevant SCF. With this notation, we can define the many-body transition amplitude from an initial state

$|\Psi_I\rangle$ to a final state $|\Psi_F\rangle$ as

$$\begin{aligned} M^{I,F} &= \langle \Psi_F | O | \Psi_I \rangle \\ &= \sum_{i}^{\text{unocc}} \sum_{j}^{\text{occ}} \left\langle \Psi_F | \Psi_I^{+i-j} \right\rangle \langle \Psi_I^{+i-j} | \hat{O} | \Psi_I \rangle \\ &= \sum_{i}^{\text{unocc}} \sum_{j}^{\text{occ}} \left\langle \Psi_F | \Psi_I^{+i-j} \right\rangle \tilde{o}_{ij}, \end{aligned} \tag{10}$$

where the functional form of O enforces that only single electron-hole pair excitations of the initial state can couple with the final state. The notation Ψ_I^{+i-j} implies the annihilation of the electron in orbital j and the creation of an electron in orbital i—a non-self-consistent creation of a single electron-hole pair within the orbitals defined by the initial state. Thus, $M^{I,F}$ can be expressed as a linear combination of purely single-particle transition amplitudes ($\tilde{o}_{ij}$) with the coefficients given by the many-body overlap terms $\langle \Psi_F | \Psi_I^{+i-j} \rangle$.

For the XES process, Ψ_I is the state with a core hole and can be approximated by the expression shown in Eq. (2). Consistently, we will employ the simplest case for the final state, Ψ_F, as representing a core-filled state with a single valence hole in orbital f, $|\Psi_F\rangle = |\Psi_F^{+0-f}\rangle$, where 0 denotes the core orbital. Due to the localized nature of the core electrons, it is reasonable to expect the core electron of Ψ_F to have negligible overlap with any electron present in Ψ_I, which lacks that core electron. Consequently, for XES, $\langle \Psi_F^{+0-f} | \Psi_I^{+i-j} \rangle \approx 0$ unless $i = 0$. This leads to the following simplification of Eq. (10):

$$M^{I,F} = \sum_{j}^{\text{occ}} \left\langle \Psi_F^{+0-f} | \Psi_I^{+0-j} \right\rangle \tilde{o}_{0j}, \tag{11}$$

where, to reiterate, we have put a tilde over the transition-matrix element, to emphasize the fact that, for XES, the initial state contains a core hole. We can expect the core-orbital subspaces of $|\Psi_F^{+0-f}\rangle$ and $|\Psi_I^{+0-j}\rangle$ to be approximately equal, for any f and j. First-order perturbation theory would support this approximation, especially due to the energy isolation of the core orbitals from the valence subspace—with perturbations scaling as the inverse of orbital energy differences. This was also observed numerically in our calculations. Therefore, in the overlap term $\langle \Psi_F^{+0-f} | \Psi_I^{+0-j} \rangle$, the core contribution, which can be approximated as unity, can be factored out and the overlap can be evaluated exclusively in terms of the valence orbitals. This is particularly useful in pseudopotential-based calculations, where only the valence KS orbitals are readily available.

For a final state $|\Psi_F\rangle$ having a hole in the fth orbital, the many-body overlap of Eq. (10) can now be written as

$$\left\langle \Psi_F^{+0-f} | \Psi_I^{+0-j} \right\rangle = {}^F C_{j,f} = [(-1)^{f+j}]^F m_{j,f} \tag{12}$$

such that

$${}^F m_{j,f} = \det \begin{bmatrix} {}^F\xi_{11} & \cdots & {}^F\xi_{1,f-1} & {}^F\xi_{1,f+1} & \cdots & {}^F\xi_{1,N} \\ \vdots & \ddots & \vdots & \vdots & \ddots & \vdots \\ {}^F\xi_{j-1,1} & \cdots & {}^F\xi_{j-1,f-1} & {}^F\xi_{j-1,f+1} & \cdots & {}^F\xi_{j-1,N} \\ {}^F\xi_{j+1,1} & \cdots & {}^F\xi_{j+1,f-1} & {}^F\xi_{j+1,f+1} & \cdots & {}^F\xi_{j+1,N} \\ \vdots & \ddots & \vdots & \vdots & \ddots & \vdots \\ {}^F\xi_{N,1} & \cdots & {}^F\xi_{N,f-1} & {}^F\xi_{N,f+1} & \cdots & {}^F\xi_{N,N} \end{bmatrix}, \tag{13}$$

where

$${}^F\xi_{q,p} = \left\langle \phi_p^F | \tilde{\phi}_q^I \right\rangle \tag{14}$$

denotes the single-particle overlap between the pth orbital of final state F and the qth orbital of initial state I. Since the initial state is assumed fixed as the core-ionized state, we drop specific reference to state I, but we retain the superscript F as the single-particle orbitals for each final state may vary, as we shall see below. From Eqs. (12) and (13), ${}^{\mathbf{F}}\mathbf{C}$ and ${}^{\mathbf{F}}\mathbf{m}$ can be recognized, respectively, as the matrix of the cofactors and minors of ${}^{\boldsymbol{F}}\boldsymbol{\xi}$, the $(N \times N)$ overlap matrix composed of the N lowest initial- and final-state valence orbitals

$${}^{\boldsymbol{F}}\boldsymbol{\xi} = \left\{ {}^F\xi_{q,p} \right\}_{q,p=1}^{N}. \tag{15}$$

We will make use of this realization later. The above expressions relied on two assumptions which we can reiterate here for clarity: (1) the many-body states are represented as single Slater determinants, which dictates that their overlap is also a determinant; and (2) a specific core orbital 0 on a single atomic site is assumed unoccupied in the initial state and occupied in the final state.

B. Orbital-optimized DFT

Within the orbital-constrained framework, the ooDFT approximation employs a fully self-consistent procedure such that a final state with filled core and a hole in the fth valence orbital is approximated by the SD:

$$|\Psi_F\rangle = |\Psi_{-f}^{(f)}\rangle = a_f^{(f)} \left(\prod_{j=1}^{N} \left(a_j^{(f)} \right)^\dagger \right) a_0^\dagger |0\rangle, \tag{16}$$

where $(a_j^{(f)})^\dagger$ is the creation operator for the jth KS orbital $\phi_j^{(f)}$ corresponding to the SCF of a system with a hole in the fth orbital, preserved, for example, using MOM. There is a distinct set of operators for each final state F.

The resulting transition amplitude is then written as

$$M^F = M^f_{\text{ooDFT}} = \left\langle \Psi_{-f}^{(f)} | \hat{O} | \Psi_{\text{I}} \right\rangle = \sum_{j=1}^{N} C_{j,f}^{(f)} \tilde{o}_{0j}, \tag{17}$$

where

$$C_{j,f}^{(f)} = \left\langle \Psi_{-f}^{(f)} | \Psi_{\text{I}}^{+0-j} \right\rangle \tag{18}$$

is the relevant determinantal overlap with $|\Psi_{\rm I}^{+0-j}\rangle = \tilde{a}_j\tilde{a}_0^\dagger|\Psi_{\rm I}\rangle$. Note that the transition moment is identical to that of the single-particle deexcitation of a noninteracting electron to the core level from an auxiliary orbital given by

$$|\phi_f^{\rm ooDFT}\rangle = \sum_{j=1}^{N} C_{j,f}^{(f)}\,|\tilde{\phi}_j\rangle\,. \tag{19}$$

For phenol, the improvement in agreement with the experimental XES line shape is apparent in Fig. 1. In the Supplemental Material (SM) [38], we provide a comparison of the range-separated and global hybrid functionals in Figs. S1 and S2 for phenol and in Figs. S3 and S4 for acetone.

C. The MBXES approach

A major drawback of the ooDFT method is that it requires a separate self-consistent field calculation for each final state of the system, rendering the computation formidably expensive, especially for large systems. Additionally, depending on the symmetry of the hole, certain configurations (especially near degeneracies) can be numerically difficult to converge.

To remedy this, we note that if the valence hole is sufficiently delocalized and, consequently, is less likely to induce a drastic change among the occupied electronic orbitals, we are justified in approximating ooDFT using a formalism which retains the self-consistent effect of the core hole in the initial state but entirely neglects that of the valence hole in the final state. For instance, a final state containing a hole in the fth (say) valence orbital is approximated in terms of the *frozen* ground-state orbitals as

$$|\Psi_F\rangle = |\Psi_{-f}\rangle = a_f\left(\prod_{j=1}^{N} a_j^\dagger\right)a_0^\dagger\,|0\rangle\,, \tag{20}$$

where $a_j^\dagger$ is the creation operator for the jth KS orbital (ϕ_j) of the ground-state SCF. Defining the relevant determinantal overlap as $C_{j,f} = \langle\Psi_{-f}|\Psi_{\rm I}^{+0-j}\rangle$, the transition amplitude is then given by

$$M_{\rm MBXES}^f = \langle\Psi_{-f}|\hat{O}|\Psi_{\rm I}\rangle = \sum_{j=1}^{N} C_{j,f}\,\langle\tilde{\phi}_0|\hat{o}|\tilde{\phi}_j\rangle\,, \tag{21}$$

with

$$|\phi_f^{\rm MBXES}\rangle = \sum_{j=1}^{N} C_{j,f}\,|\tilde{\phi}_j\rangle \tag{22}$$

representing the corresponding auxiliary orbital. Note that since we now construct each $|\Psi_F\rangle$ from the frozen ground-state KS orbitals, the many-body overlap of Eq. (10), which in the ooDFT approximation is given by $C_{j,f}^{(f)}$ [Eq. (18)], becomes independent of the SCF of the specific final state, indexed by F and thereby representable as $C_{j,f}$, without any superscript. Likewise, the single-particle overlaps [see Eq. (14)] are independent of F and can be written as ${}^F\xi_{p,q} = \xi_{p,q}$.

We dub this approximation the many-body X-ray emission spectroscopy (MBXES) method by direct analogy with a similar approach used for x-ray absorption [39–41]. The similarity between ooDFT (blue) and MBXES (green) plots in Fig. 1 justifies the underlying approximation for these cases.

Unlike ooDFT, the MBXES method requires only two SCF calculations: one with a core hole (for the initial state) and one without (for all final states). It also avoids instabilities resulting from the near degeneracy of orbitals. Additionally, unlike the response-based approaches, it can be used in plane-wave calculations in conjunction with pseudopotentials, where a modification in the pseudopotential incorporates the effects of the core hole and thereby eliminates the need for any additional charge-constraining technique. As shown in Fig. S6, the O $K\,\alpha$ MBXES spectrum of C_6H_5OH calculated using Q-CHEM, an all-electron software package employing localized basis functions, compares well with that calculated using the pseudopotential-based plane-wave software QUANTUM ESPRESSO [42].

It is also worth noting in Fig. 1 (and as we shall see later in Sec. IV F and in the SM) the good agreement between the deexcitation energies of ooDFT (whose energies are computed self-consistently) and MBXES [derived from the ground state (GS) KS eigenvalues]. For the particular functional and these systems, this implies that the KS eigenvalues are good approximations to the quasiparticle excitation energies—although there will obviously be cases, outside the examples we report, where increased accuracy can be provided by better functionals or perturbative approaches such as the *GW* approximation [43,44].

To illustrate the accuracy of the more efficient MBXES approach vs adiabatic LR-TDDFT, we provide multiple examples for the XES of small molecules in Fig. 2 where the corresponding change in dipole moment is also provided. Note that, consistent with the discussion presented earlier, in general, a larger change in the valence electrostatic dipole moment upon core ionization results in a larger difference between the two spectra, with the former typically showing better agreement with experiment. For example, for C_6H_5OH (spectra also presented in the bottom panel of Fig. 1), which corresponds to a relatively large change (3.01 D) in the electrostatic dipole moment, the penultimate peak at 527.5 eV in the adiabatic LR-TDDFT spectrum is seen to be the most intense. On the other hand, in the MBXES, ooDFT, and experimental spectra, which show appreciable mutual agreement in the relative intensity of the peaks, the third peak from the right-hand side (at 525.1 eV for the experimental spectrum and at 525.5 eV for the ooDFT and MBXES spectra) has the highest intensity. It is to be noted that, although the simulated spectrum, especially the deexcitation energies, depend, to some extent, on the exchange-correlation functional and can therefore be made to agree better with experiments by using improved functionals, the oscillator-strength accuracy, which is our primary focus here, is definitely improved over LR-TDDFT by the orbital-constrained approaches. Conversely, for CH_3Cl (spectra also presented in the top panel of Fig. 1), which corresponds to a much smaller change (1.43 D) of the electrostatic dipole moment, all of the spectra show an intense peak around 2817 eV and a shorter but broader feature at a lower energy of 2814 eV.

Molecule	ΔD	Spectra	Molecule	ΔD	Spectra
C_6H_5F [F K α]	3.28	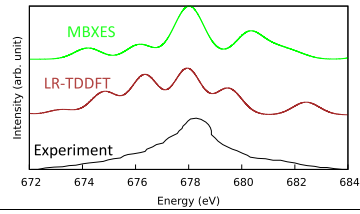	CH_3Cl [Cl K β]	1.43	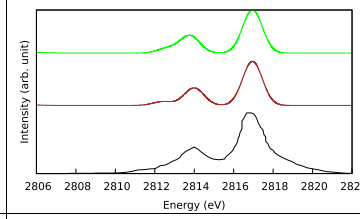
C_6H_5OH [O K α]	3.01	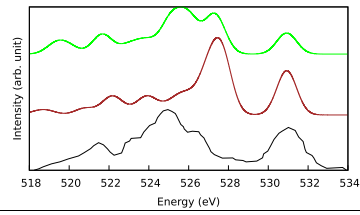	H_2S [S K β]	0.74	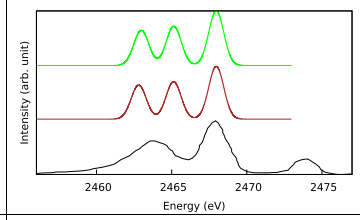
$(CH_3)_2SO$ [O K α]	2.72	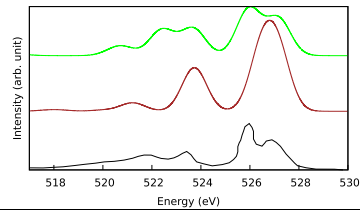	NH_3 [N K α]	0.45	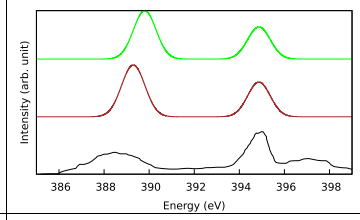
$(CH_3)_2CO$ [O K α]	2.57	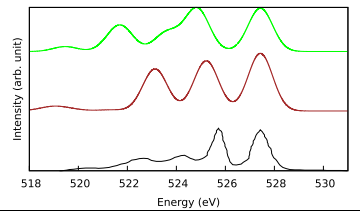	CH_3OH [O K α]	0.3	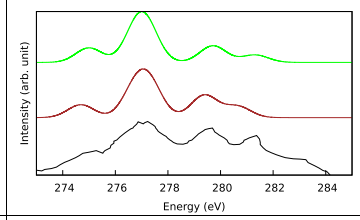
CF_3Cl [Cl K β]	1.75	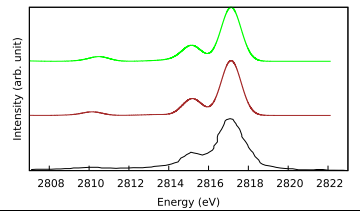	C_6H_5OH [Valence De-excitation from initial state with hole in 11th KS orbital]	0.17	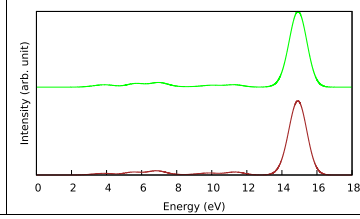

FIG. 2. Table showing experimental [32,33,45–48] (black) adiabatic LR-TDDFT (brown) and MBXES (green) spectra of different molecules. The second column shows the change in the electrostatic dipole moment, in Debye units, of the remaining electrons following the relevant core ionization.

D. Single-particle approximations

1. Projected ground state

Further approximations, sacrificing accuracy in lieu of computational efficiency, can be made beyond MBXES. For example, we propose the projected ground-state (pGS) approximation, which takes into account the change in the participating valence orbital in response to the core-hole filling, but ignores the same for the other (spectator) orbitals.

From Eq. (21) the MBXES transition dipole moment is given by

$$M^f_{\mathrm{MBXES}} = \sum_{j=1}^{N} C_{j,f}\tilde{o}_{0j}.$$

Now, if we approximate the determinantal overlap with the relevant single-particle counterpart,

$$\begin{aligned} C_{j,f} &= \langle \Psi_{-f}|\Psi_{\mathrm{I}}^{+0-j}\rangle \\ &= \langle \Psi_{\mathrm{GS}}|a_f^\dagger \tilde{a}_j|\Psi_{\mathrm{I}}^{+0}\rangle \\ &\approx \langle \phi_f|\tilde{\phi}_j\rangle^* \\ &= \xi^*_{j,f}, \end{aligned} \tag{23}$$

then, the transition dipole moment becomes

$$M^f_{\mathrm{pGS}} = \sum_{j=1}^{N} \xi^*_{j,f}\tilde{o}_{0j}, \tag{24}$$

while $|\phi_f^{\mathrm{pGS}}\rangle = \sum_{j=1}^{N} \xi^*_{jf}\,|\tilde{\phi}_j\rangle$ gives the corresponding auxiliary orbital.

TABLE I. Table summarizing important properties and approximations corresponding to various simulation methods discussed in the paper. Note that, in each case, the transition-dipole moment is given by $\langle \text{core}|\hat{o}|\text{auxiliary orbital}\rangle$, where $\hat{o}$ is the single-particle dipole operator.

Method	Final orbitals consistent with valence hole	Relaxation of spectator electronic orbitals	Initial orbitals consistent with core hole	Auxiliary orbital
ooDFT	Yes	Yes	Yes	$\sum_{j=1}^{N} C_{j,f}^{(f)} \lvert\tilde{\phi}_j\rangle$
MBXES	No	Yes	Yes	$\sum_{j=1}^{N} C_{j,f} \lvert\tilde{\phi}_j\rangle$
pGS	No	No	Yes	$\sum_{j=1}^{N} \xi_{jf}^{*} \lvert\tilde{\phi}_j\rangle$
GS	No	No	No	$\sum_{j=1}^{\text{all}} \xi_{jf}^{*} \lvert\tilde{\phi}_j\rangle$

Significant computational savings arise here due to replacing the N-electron determinant with a single overlap matrix element. In terms of the physical approximation involved, pGS takes into account the fact that the participating orbital (i.e., the valence orbital from which the electronic deexcitation takes place) should be different in the presence and in the absence of the core hole. What is missing in the pGS approximation is the explicit inclusion of relaxation of the other valence electrons. In general, absorption spectra calculated with the pGS approximation [38], show good agreement with MBXES spectra, despite this simplification.

2. Ground state

Note that in all of the aforementioned approximations, separate sets of orbitals $\{\tilde{\phi}_j\}$ and $\{\phi_j\}$ (or $\{\phi_j^{(f)}\}$) are used for the initial and the final state, indicating separate SCFs for states with and without a core hole. As a final approximation within the orbital-constrained framework, we now neglect this effect by extending the sum in Eq. (24) to all orbitals, thereby approximating the transition moment entirely within a *ground-state single-particle* (GS) treatment as follows:

$$\begin{aligned}\left(M_{\text{GS}}^{f}\right)^{*} &= \sum_{j=1}^{\text{all}} \xi_{jf}\, \langle\tilde{\phi}_j|\hat{o}|\tilde{\phi}_0\rangle \\ &= \langle\phi_f| \sum_{j=1}^{\text{all}} |\tilde{\phi}_j\rangle\, \langle\tilde{\phi}_j|\hat{o}|\tilde{\phi}_0\rangle \\ &= \langle\phi_f|\hat{o}|\tilde{\phi}_0\rangle \approx \langle\phi_f|\hat{o}|\phi_0\rangle\,, \end{aligned} \tag{25}$$

where the approximation that the core orbital remains unchanged, $|\phi_0\rangle \approx |\tilde{\phi}_0\rangle$, is validated by our calculations showing $\langle\phi_0|\tilde{\phi}_0\rangle \approx 1$. A table summarizing the different approximations within the framework of orbital-constrained XES is presented in Table I.

3. Relation between M_{MBXES}^{f} and M_{GS}^{f}

It is instructive to investigate analytically the conditions for equivalence of the GS and the MBXES spectra. To this end, we aim to find the linear-algebraic relation between the MBXES coefficients ($\{C_{i,j}\}$) and the single-particle overlaps($\{\xi_{i,j}\}$). The inverse of the lowest $N \times N$ overlap matrix can be related to its matrix of cofactors as

$$\boldsymbol{\xi}^{-1} = \frac{\text{adj}(\boldsymbol{\xi})}{\det(\boldsymbol{\xi})} = \frac{\boldsymbol{C}^{T}}{\det(\boldsymbol{\xi})}. \tag{26}$$

So, for each matrix element,

$$\left(\boldsymbol{\xi}^{-1}\right)_{f,j} = \frac{C_{j,f}}{\det(\boldsymbol{\xi})}. \tag{27}$$

Therefore, if the $(N \times N)$ matrix $\boldsymbol{\xi}$ is orthogonal (i.e., if its transpose is equal to its inverse), then, noting that the determinant of an orthogonal matrix is ± 1, we obtain

$$\xi_{j,f}^{*} = \pm C_{j,f}, \tag{28}$$

and so, ignoring the ambiguity in sign,

$$\left(M_{\text{MBXES}}^{f}\right)^{*} \approx \sum_{j=1}^{N} \xi_{j,f}\, \langle\tilde{\phi}_j|\hat{o}|\tilde{\phi}_0\rangle\,, \tag{29}$$

which is the projected ground-state approximation. And, furthermore, if the overlap matrix $\boldsymbol{\xi}$ is truly orthogonal, then this implies that the initial- and final-state occupied subspaces overlap perfectly and $\xi_{j,f} = 0$ for $j > N; f \leqslant N$. So, we can extend the sum above over all j and obtain

$$\left|M_{\text{MBXES}}^{f}\right|^{2} = |M_{\text{GS}}^{f}|^{2}. \tag{30}$$

To reiterate, this is a remarkable simplification, which can be restated as follows: If the electrons occupy the same space in the ground and the core-excited state, then the GS and the MBXES spectra will be identical. Thus, the GS approach is likely to be inaccurate if the core ionization induces a large change in the valence electron density. Changes in electronic density in response to perturbations are proportional to the electronic polarizability, and so the associated polarization response seems like an appropriate metric for assessing this equivalence between GS and MBXES spectral intensity.

This is reflected in Fig. 3, which displays the GS and the MBXES spectra for CH_3Cl Cl $K\,\beta$ and C_6H_5OH O $K\,\alpha$ emission. In order to facilitate comparison, for each system the GS spectrum is scaled by a constant factor to match the intensity of the last peak, which essentially amounts to equating the oscillator strengths of the highest-energy transition. Figure 3 reveals that for CH_3Cl the two spectra are nearly coincident, which is not the case for C_6H_5OH, indicating, for the latter, a disagreement among the relative oscillator strengths of the different transitions computed within the GS and the MBXES approximation. In accordance with the aforementioned analytical argument, this disagreement can be attributed to the larger change in valence electronic polarization in C_6H_5OH.

For context, the most common practice of using valence-projected density of states to interpret XES [49–52] is yet a further approximation that ignores the single-particle matrix elements.

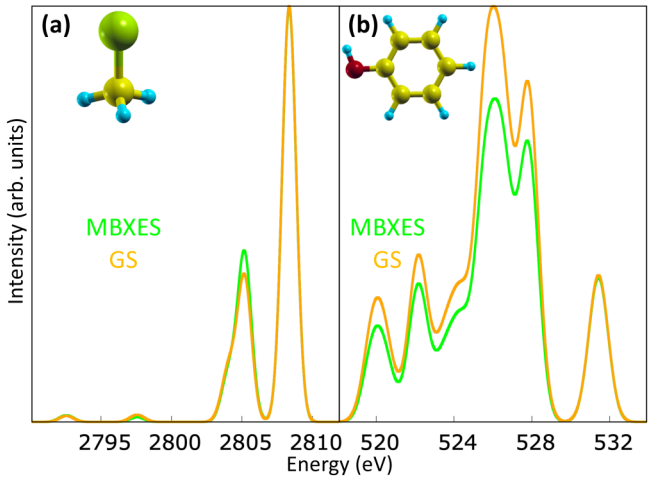

FIG. 3. Emission spectra calculated using the MBXES (green line) and the GS (orange line) approach. Panel (a) shows Cl $K\beta$ emission from CH_3Cl, which is associated with a 1.43 Debye change in valence dipole moment, while panel (b) shows O $K\alpha$ emission from C_6H_5OH, for which the valence dipole moment changes by 3.01 D. Yellow, cyan, red, and green spheres denote C, H, O, and Cl atoms, respectively. Each GS spectrum has been multiplied by a constant factor so that the intensity corresponding to the highest-energy peak matches the MBXES counterpart.

We emphasize here that, even though the inaccuracies of the adiabatic LR-TDDFT and the GS formalism can be associated with the same metric, they, in fact, stem from quite different effects. In the former, the drawback lies in a partial description of the *final* (core-filled) state while in the latter it can be attributed to a complete neglect of the *initial* (core-ionized) state effects. However, in both cases, the shortcoming lies in the inability to adequately account for the difference between the valence electronic structure of the initial and the final state. Therefore, the aforementioned metric, which provides a measure for this difference, is applicable for both of these diverse approaches.

E. Auxiliary orbitals

The auxiliary orbitals can provide a visual justification for the similarity/difference in the spectra seen in Fig. 1. As a representative example, in Fig. 4 we show the auxiliary orbitals corresponding to the 11th deexcitation in CH_3Cl (Cl $K\beta$) and the 23rd deexcitation in C_6H_5OH (O $K\alpha$) (see also Fig. S1). While for CH_3Cl, all three orbitals are in good agreement, for C_6H_5OH noticeable differences can be spotted in the auxiliary orbital obtained using LR-TDDFT. Note, however, that all three auxiliary orbitals on the right-hand-side panels are qualitatively similar, indicating that they contain appreciable contribution from the same set of constituent initial state orbitals (see also Fig. S5 in the SM which shows a bar plot of the coefficients of the contributing initial-state orbitals). However, as a consequence of the initial-state bias, $\phi_{23}^{\mathrm{TDDFT}}$ is skewed toward the core hole on the oxygen atom, while the ooDFT and MBXES counterparts display more delocalized nature. As expected, this leads to a difference in the associated oscillator strengths.

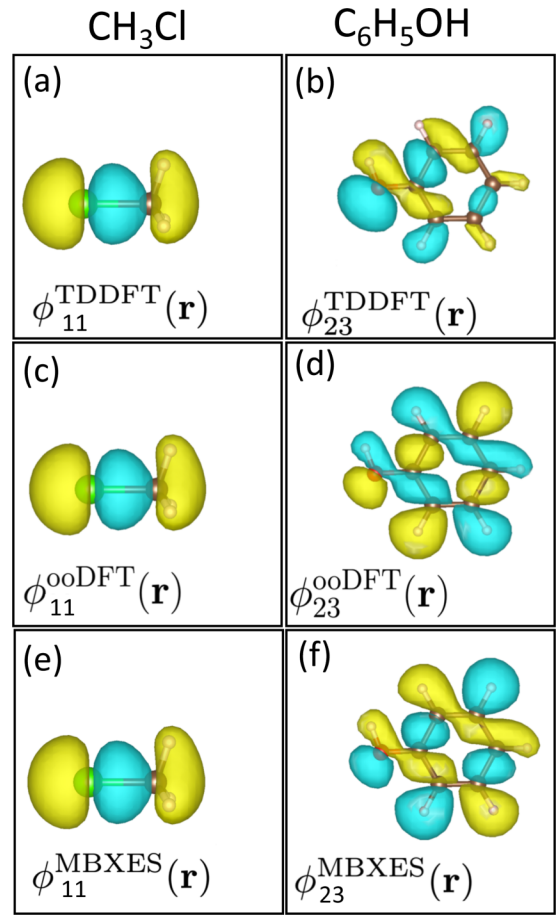

FIG. 4. Panels (a), (c), and (e) display the auxiliary orbital, evaluated using, respectively, LR-TDDFT, ooDFT, and MBXES associated with the 11th deexcitation in the Cl $K\beta$ emission of CH_3Cl. Panels (b), (d), and (f) plot the same for the 23rd deexcitation in the O $K\alpha$ emission of C_6H_5OH. These plots demonstrate that MBXES effectively approximates ooDFT while, for phenol, LR-TDDFT exhibits errors associated with the adiabatic approximation.

F. Extension to valence deexcitations

By contrast with XES, for the majority of low energy valence electronic transitions, the response-based methods have proven to be highly successful for decades [53]. In reference to the metric introduced above, it is worth noting that, in most cases, such transitions are usually associated with a comparatively small change in the polarization owing to the relatively delocalized nature of the valence hole (compared to the atomic core hole). As an illustrative example, in Fig. 5, we plot the simulated emission spectra of C_6H_5OH associated with deexcitation from an initial state with a hole in the 11th (valence) KS orbital. Owing to the small (0.17 D) change in the electrostatic dipole moment, the LR-TDDFT result is found to be in excellent agreement with the ooDFT and the MBXES counterparts. In contrast, the charge-transfer excitation, which is accompanied by an appreciable spatial separation of charges resulting typically in a large change in the valence polarization, is a well-documented example of the failure of adiabatic LR-TDDFT in predicting the excitation energy [54,55], although further studies are needed to investigate the accuracy in the calculation of oscillator strength.

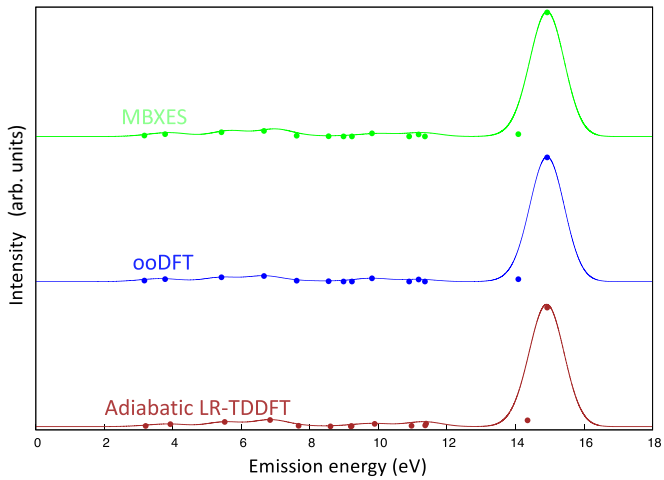

FIG. 5. Simulated emission spectra, computed with MBXES, ooDFT, and adiabatic LR-TDDFT, corresponding to electronic deexcitation of C_6H_5OH from an initial state with a hole in the 11th KS valence orbital. The associated change in valence polarization is 0.17 D.

V. CONCLUSIONS

In summary, with a focus on valence-to-core electronic deexcitation, we use a generalized formalism to link the disparate response-based and orbital-constrained approaches, which are the two standard pathways for modeling electronic excited states starting from DFT calculations. Our analytical and computational results show that, unless the deexcitation induces a small change in the valence polarization, the popular adiabatic approximation of the response-based approach might incur significant inaccuracies in the oscillator strength. Consequently, such a change in polarization can be used as an effective metric for assessing the validity of the adiabatic approximation. In fact, a valence-to-core deexcitation can often render the adiabatic approximation inadequate since the filling of a localized core orbital may lead to appreciable rearrangement of the valence electrons. The aforementioned shortcoming is not present in the orbital-constrained approach such as ooDFT, which typically yields accurate results. By modifying the ooDFT formalism with physically motivated approximations, we propose a flexible computational technique, MBXES, which can simulate oscillator strengths accurately at a much lower computational cost.

ACKNOWLEDGMENTS

This research was supported by the Director, Office of Science, Office of Basic Energy Sciences, of the U.S. Department of Energy under Contract No. DE-AC02-05CH11231. S.R. and D.P. acknowledge the support of Molecular Foundry, LBNL. Computational works were performed on the TMF supercomputing facility managed by the High Performance Computing Services Group at LBNL. M.H.-G. is a part owner of Q-CHEM, which is the software platform in which the computations described here were carried out.

[1] P. Hohenberg and W. Kohn, Phys. Rev. **136**, B864 (1964).
[2] W. Kohn and L. J. Sham, Phys. Rev. **140**, A1133 (1965).
[3] A. D. Becke, J. Chem. Phys. **140**, 18A301 (2014).
[4] R. O. Jones, Rev. Mod. Phys. **87**, 897 (2015).
[5] D. J. Tozer and M. J. G. Peach, Phys. Chem. Chem. Phys. **16**, 14333 (2014).
[6] T. van Mourik, M. Bühl, and M.-P. Gaigeot, Philos. Trans. R. Soc. A **372**, 20120488 (2014).
[7] D. Hait and M. Head-Gordon, J. Phys. Chem. Lett. **12**, 4517 (2021).
[8] J. Cullen, M. Krykunov, and T. Ziegler, Chem. Phys. **391**, 11 (2011).
[9] F. A. Evangelista, P. Shushkov, and J. C. Tully, J. Phys. Chem. A **117**, 7378 (2013).
[10] G. Levi, A. V. Ivanov, and H. Jónsson, J. Chem. Theory Comput. **16**, 6968 (2020).
[11] P. Ramos and M. Pavanello, J. Chem. Phys. **148**, 144103 (2018).
[12] C.-L. Cheng, Q. Wu, and T. Van Voorhis, J. Chem. Phys. **129**, 124112 (2008).
[13] S. Roychoudhury, S. Sanvito, and D. D. O'Regan, Sci. Rep. **10**, 8947 (2020).
[14] M. Petersilka, U. J. Gossmann, and E. K. U. Gross, Phys. Rev. Lett. **76**, 1212 (1996).
[15] M. E. Casida, Time-dependent density functional response theory for molecules, in *Recent Advances in Density Functional Methods* (World Scientific, Singapore, 1995), pp. 155–192.
[16] E. L. Shirley, Phys. Rev. Lett. **80**, 794 (1998).
[17] M. Rohlfing and S. G. Louie, Phys. Rev. B **62**, 4927 (2000).
[18] M. Odelius, Phys. Rev. B **79**, 144204 (2009).
[19] R. Guillemin, S. Carniato, L. Journel, W. C. Stolte, T. Marchenko, L. E. Khoury, E. Kawerk, M. N. Piancastelli, A. C. Hudson, D. W. Lindle, and M. Simon, J. Electron Spectrosc. Relat. Phenom. **188**, 53 (2013).
[20] S. Roychoudhury, Z. Zhuo, R. Qiao, L. Wan, Y. Liang, F. Pan, Y.-d. Chuang, D. Prendergast, and W. Yang, ACS Appl. Mater. Interfaces **13**, 45488 (2021).
[21] T. A. Pascal, U. Boesenberg, R. Kostecki, T. J. Richardson, T.-C. Weng, D. Sokaras, D. Nordlund, E. McDermott, A. Moewes, J. Cabana, and D. Prendergast, J. Chem. Phys. **140**, 034107 (2014).
[22] F. de Groot, Chem. Rev. **101**, 1779 (2001).
[23] U. Bergmann and P. Glatzel, Photosynth. Res. **102**, 255 (2009).
[24] A. A. E. Fouda and N. A. Besley, J. Comput. Chem. **41**, 1081 (2020).
[25] M. W. D. Hanson-Heine, M. W. George, and N. A. Besley, J. Chem. Phys. **146**, 094106 (2017).
[26] A. T. B. Gilbert, N. A. Besley, and P. M. W. Gill, J. Phys. Chem. A **112**, 13164 (2008).
[27] Assuming the core is filled in all constituent SDs.
[28] We drop the I superscript on M as the initial state, which is the core-ionized state, will be the same for all deexcitations in XES.
[29] S. Hirata and M. Head-Gordon, Chem. Phys. Lett. **314**, 291 (1999).

[30] X. Ge, A. Calzolari, and S. Baroni, Chem. Phys. Lett. **618**, 24 (2015).
[31] E. Rebolini and J. Toulouse, J. Chem. Phys. **144**, 094107 (2016).
[32] D. W. Lindle, P. L. Cowan, T. Jach, R. E. LaVilla, R. D. Deslattes, and R. C. C. Perera, Phys. Rev. A **43**, 2353 (1991).
[33] V. D. Yumatov, A. V. Okotrub, G. G. Furin, and N. F. Salakhutdinov, Russ. Chem. Bull. **46**, 2074 (1997).
[34] E. Epifanovsky, A. T. B. Gilbert, X. Feng, J. Lee, Y. Mao, N. Mardirossian, P. Pokhilko, A. F. White, M. P. Coons, A. L. Dempwolff *et al.*, J. Chem. Phys. **155**, 084801 (2021).
[35] N. Mardirossian and M. Head-Gordon, J. Chem. Phys. **144**, 214110 (2016).
[36] D. E. Woon and T. H. Dunning, J. Chem. Phys. **98**, 1358 (1993).
[37] R. A. Kendall, T. H. Dunning, and R. J. Harrison, J. Chem. Phys. **96**, 6796 (1992).
[38] See Supplemental Material at http://link.aps.org/supplemental/10.1103/PhysRevB.106.075133 for simulated examples.
[39] Y. Liang, J. Vinson, S. Pemmaraju, W. S. Drisdell, E. L. Shirley, and D. Prendergast, Phys. Rev. Lett. **118**, 096402 (2017).
[40] Y. Liang and D. Prendergast, Phys. Rev. B **97**, 205127 (2018).
[41] Y. Liang and D. Prendergast, Phys. Rev. B **100**, 075121 (2019).
[42] P. Giannozzi, S. Baroni, N. Bonini, M. Calandra, R. Car, C. Cavazzoni, D. Ceresoli, G. L. Chiarotti, M. Cococcioni, I. Dabo, A. D. Corso, S. de Gironcoli *et al.*, J. Phys.: Condens. Matter **21**, 395502 (2009).
[43] M. S. Hybertsen and S. G. Louie, Phys. Rev. B **34**, 5390 (1986).
[44] L. Hedin and S. Lundqvist, *Effects of Electron-Electron and Electron-Phonon Interactions on the One-Electron States of Solids*, edited by F. Seitz, D. Turnbull, and H. Ehrenreich, Solid State Physics (Academic Press, New York, 1970), Vol. 23, pp. 1–181.
[45] K. M. Lange and E. F. Aziz, Chem. Soc. Rev. **42**, 6840 (2013).
[46] R. Mayer, D. W. Lindle, S. H. Southworth, and P. L. Cowan, Phys. Rev. A **43**, 235 (1991).
[47] J. Nordgren, H. Agren, L. O. Werme, C. Nordling, and K. Siegbahn, J. Phys. B **9**, 295 (1976).
[48] J.-E. Rubensson, N. Wassdahl, R. Brammer, and J. Nordgren, J. Electron Spectrosc. Relat. Phenom. **47**, 131 (1988).
[49] T. V. Vu, A. Lavrentyev, B. Gabrelian, V. Tkach, K. D. Pham, O. Marchuk, O. Parasyuk, and O. Khyzhun, Solid State Sci. **104**, 106287 (2020).
[50] D. R. Mortensen, G. T. Seidler, J. J. Kas, N. Govind, C. P. Schwartz, S. Pemmaraju, and D. G. Prendergast, Phys. Rev. B **96**, 125136 (2017).
[51] W. T. Hong, K. A. Stoerzinger, B. Moritz, T. P. Devereaux, W. Yang, and Y. Shao-Horn, J. Phys. Chem. C **119**, 2063 (2015).
[52] G. B. Grad, E. R. González, J. Torres Díaz, and E. V. Bonzi, J. Mater. Sci. Res. Rev. **1**, 1 (2018).
[53] M. R. Silva-Junior, M. Schreiber, S. P. A. Sauer, and W. Thiel, J. Chem. Phys. **129**, 104103 (2008).
[54] A. Dreuw, G. R. Fleming, and M. Head-Gordon, J. Phys. Chem. B **107**, 6500 (2003).
[55] A. Dreuw and M. Head-Gordon, J. Am. Chem. Soc. **126**, 4007 (2004).